Proceedings of IMECE2009
2009 ASME International Mechanical Engineering Congress and Exposition
November 13-19, 2009, Lake Buena Vista, Florida, USA

IMECE2009-13024

DRAFT

SLIDING MODE CONTROLLER AND FILTER APPLIED TO A PNEUMATIC MCKIBBEN MUSCLE ACTUATOR

V. Jouppila
Department of Mechanics and Design
Tampere University of Technology
33101 Tampere, Finland
ville.jouppila@tut.fi

S. A. Gadsden
Department of Mechanical Engineering
McMaster University
Hamilton, Ontario, Canada L8S 4L7
gadsdesa@mcmaster.ca

S. R. Habibi
Department of Mech. Eng.
McMaster University, Hamilton,
Ontario, Canada L8S 4L7
habibi@mcmaster.ca

G. M. Bone
Department of Mech. Eng.
McMaster University, Hamilton,
Ontario, Canada L8S 4L7
gary@mcmaster.ca

A. Ellman
Dept. of Mechanics and Design
Tampere University of Technology
33101 Tampere, Finland
asko.ellman@tut.fi

ABSTRACT

In this paper, a robust and stable control strategy is applied to a Festo fluidic muscle actuator, with the objective of trajectory following control. A complete model of this system is not available which leads to unmodeled dynamics and uncertainties. Furthermore, full-state feedback is required for this type of control. However, in practice not all of the states are measured or available due to cost or availability of instruments, thus a full-state observer is required. The Smooth Variable Structure Filter (SVSF) is a relatively new predictor-corrector method used for state and parameter estimation, and has a form that is able to provide full-state information. In this regard, a new strategy that combines Sliding Mode Control (SMC) with the SVSF is used to control this system. The estimated states from the SVSF are used by the sliding mode controller to obtain a discontinuous control signal. This signal drives the plant to follow a desired state trajectory required by the pneumatic McKibben muscle actuator. Simulation results were generated based on a realistic desired trajectory. The results of the SMC-SVSF control strategy are compared with a tuned PID controller. The described control strategy is able to overcome the nonlinearities present in the system, has a fast response time, and is robust and stable to modeling uncertainties and measurement noise.

KEYWORDS

McKibben muscle actuator, sliding mode control, smooth variable structure filter, trajectory following.

INTRODUCTION

Pneumatic actuators are commonly avoided for advanced applications due to problems with control caused by the compressibility of air and other nonlinear effects. Pneumatic control systems are mainly used in simple industrial applications with limited requirements for accurate control of motion and force. However, high power-to-weight ratios, compactness, ease of maintenance, and the safety of pneumatic actuators, offer desirable features for many industrial designs. The pneumatic McKibben muscle actuator is a new type of actuator that offers a high power-to-weight performance and is able to operate in a wide range of environments. The compressibility of air, the nonlinear air flow characteristics through the valves, and the nonlinear characteristics of the McKibben muscle actuator result in a complex and difficult system to model and control.

A brief review of literature demonstrates that a large number of control strategies have been proposed to handle the effects of the nonlinearities present in the muscle actuator. These include the following: PID implementation [1], adaptive control strategies [2–5], nonlinear optimal predictive control [6], variable structure systems [7, 8], gain scheduling [9], neural networks [10], and neuro-fuzzy/genetic control methods [11–15]. Furthermore, other studies have shown sliding mode controllers applied to pneumatic muscle actuators [16–21]. Sliding mode control (SMC) is a form of variable structure control (VSC) [22]. It is commonly implemented for the control of nonlinear systems, and can provide accurate tracking with a bounded error in the presence of parameter variations and model uncertainties [22, 23]. Since the system structure is highly nonlinear and not completely known, the SMC strategy was chosen for the control of the system.

In recent years, a considerable amount of research has been performed to develop inexpensive servo-pneumatic systems using PWM-driven on/off solenoid valves. In a PWM-controlled system, the power is delivered to the actuator in discrete packets of fluid mass, as the valve is either completely on or off. However, if the switching frequency of the valve is significantly higher than the system dynamics, the system will act as a low-pass filter responding similarly as for continuous mass flow. The development of an analytical dynamic model of the system is difficult, and often prevents the direct use of analytical control designs.

Although previous work has shown the potential of PWM-controlled pneumatics, they have suffered due to the lack of an analytical approach for analyzing the system [24–27]. However, some effort has been made in the area of analytical modeling of such systems [28–30]. In one article, the nonlinearities of the system were handled by proposing a switching controller based on the reduced order nonlinear model of the system [31]. Another notable paper introduced an experimentally developed discrete-time model of a PWM-controlled pneumatic servo system, for which a controller was developed based on discrete-time control methods [32]. Another strategy used a linear state-space averaged model and a linear robust controller based on a loop shaping approach was introduced [33]. This approach was later followed by a nonlinear averaged model and a sliding mode controller design [34, 35]. A linearization approach was later used in an attempt to remove the need for complicated nonlinear controllers [36].

The overall system is highly nonlinear and not completely known leading to unmodeled uncertainties. Furthermore, full-state feedback is required for the control strategy to be implemented. However, in practice not all of the states are measured or available due to cost or availability of instruments. Hence, a full-state observer based on the Smooth Variable Structure Filter (SVSF) has been used [37]. The SVSF is a relatively new predictor-corrector method used for state and parameter estimation, and has a form that is able to provide full-state information. In this regard, a new strategy that combines SMC with the SVSF is used to control this system. The estimated states from the SVSF are used by the sliding mode controller to obtain a discontinuous control signal for the valve. This control strategy is able to overcome the nonlinearities present in the system, has a fast response time, and is robust and stable to modeling uncertainties and noise.

SYSTEM MODELING

System Setup and Structure

The system hardware is illustrated schematically in Fig. 1. The Festo fluidic muscle (MAS10-300 mm) is hanging vertically, actuating (lifting) the attached payload. The supply pressure (0.65 MPa abs.) for the system is provided by the proportional pressure regulator (Festo VPPM-6L-L1-G18-0L6H-V1N). A 3/2 high switching on/off solenoid valve (Festo MHE2-1/8-MS1H-3/2G-M7) is controlled to actuate the muscle actuator and the payload. The controller is implemented in a DSpace and Matlab Simulink environment and provides the pulsed valve control signal. An electronic amplifier is used to provide sufficient power to actuate the valve. Flow control valves were added between the on/off solenoid valve and the muscle actuator to filter out the pressure vibrations caused by the pulsing of the solenoid valve. A pressure sensor (Festo SDE1-D6-G2-H18-C-PU-M8) provides a feedback signal for the controller. The displacement of the actuator and payload is measured by an electrical potentiometer.

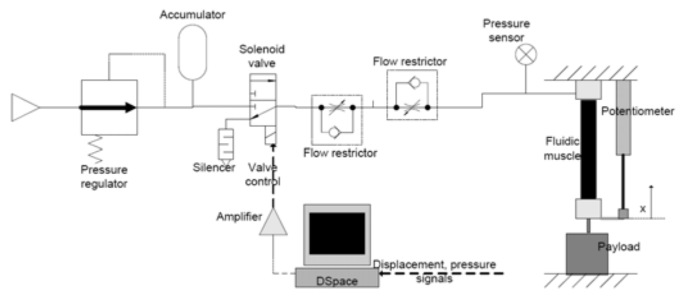

Fig. 1. System hardware

McKibben Muscle Actuator

The McKibben muscle is an actuator that consists of a rubber tube with a non-extensible fiber surrounding [38]. This physical configuration causes the muscle to have variable-stiffness spring-like characteristics, nonlinear passive elasticity, physical flexibility, and very light weight compared to other types of artificial actuators [39]. The Festo fluidic muscle differs slightly from the general McKibben type muscle. The fiber of the fluidic muscle is knit in the tube, offering easy assembly and improved hysteretic behavior and nonlinearity compared to conventional designs [40].

During pressurization of the muscle with compressed air, the muscle widens in diameter and shortens in longitudinal direction. The maximum force is gained at the beginning of the contraction and decreases with increasing contraction [38]. The actuator is unidirectional and its maximum contraction without load is typically 20% to 25%. The nominal force-to-contraction at different pressure levels is highly nonlinear, and adds to the difficulty of effectively modeling the muscle actuator. As with all actuation systems, effective design with pneumatic muscle actuators relies on being able to accurately model and predict the forces that will be generated under any operating conditions. In general, the properties of the muscle actuator depend on the geometric parameters shown in Fig. 2.

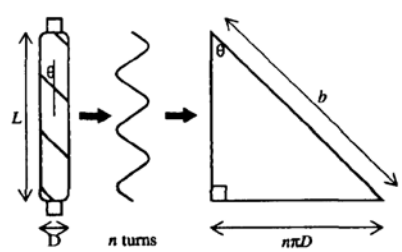

Fig. 2. Geometric model of McKibben actuator [39]

From the geometry of the muscle, the overall length of the actuator and the diameter are given by the following two equations:

$$L = b\cos\theta \tag{1}$$

$$D = \frac{b \sin \theta}{n \pi} \tag{2}$$

Where b is the length of one braid strand, considered to be inextensible, and n is the number of times a strand encircles the muscle's circumference from end-cap to end-cap. Assuming an ideal cylindrical shape, the enclosed volume is defined as follows:

$$V = \frac{b^3}{4\pi n^2} \cos\theta \sin^2\theta \tag{3}$$

From the principle of virtual work and conservation of energy, the following is the work required to deform the muscle membrane (assuming quasi-static conditions):

$$F = -p \frac{dV}{dL} \tag{4}$$

Substitution of equation (3) into (4) leads to the force generation equation, first proposed in [41]:

$$F = \frac{\pi D_0^2 p}{4} (3\cos^2\theta - 1) \tag{5}$$

Where F is the contractile muscle force, D_0 is the diameter of the actuator at the braid angle of 90° (theoretical maximum), and p is the muscle pressure. The same force equation was given in a more useful form as follows [42, 17]:

$$\begin{gathered} F = \left(\pi r_0^2\right) p [a(1-\varepsilon)^2 - b] \\ a = \frac{3}{\tan^2\theta_0} \quad b = \frac{1}{\sin^2\theta_0} \quad \varepsilon = \frac{l_0 - l}{l_0} \end{gathered} \tag{6}$$

Where r_0 and θ_0 are respectively the minimum radius and braid angle, l_0 is the maximum length, and ε is contraction ratio. Equations (5) and (6) give a basis for predicting the generated muscle force. However, they fail to completely model the behaviour of braided muscle actuators due to the assumption of lossless operation. Subsequently, various hypotheses have been developed to account for the effects of tubing elasticity, internal frictions, braid thickness, stretching of the fibres, end cap diameter (not cylindrical) and material modeling in order to provide more accurate models [38, 39, 42–45]. Despite the improvements, errors between the predicted and measured force still exists. Especially in the case of Festo fluidic muscles, the models have been too inaccurate leading to a use of various corrective factors and exponential curve fitting methods [17, 46]. In this paper, an alternative force model is introduced. At the maximum possible constant pressure (0.6 MPa in this case); the maximum force depends nonlinearly on the muscle contraction. A third-order polynomial fit can be introduced to describe this relationship, as follows:

$$F_{\max}(x) = a_0 + a_1 x + a_2 x^2 + a_3 x^3 \tag{7}$$

When the muscle displacement is held constant, the actuator force depends almost linearly on the pressure. Thus, a factor to describe the force per unit pressure as a function of the muscle displacement is introduced:

$$F_{muscle} = F_{\max}(x) - (p_{\max} - p_m)(\frac{k_0 - k_1 x}{k_2}) \tag{8}$$

Where p_{max} is the maximum available muscle pressure and p_m is the measured muscle pressure. Coefficients k_0 [N], k_1 [N/m] k_2 [Pa] are found by using least squares methods.

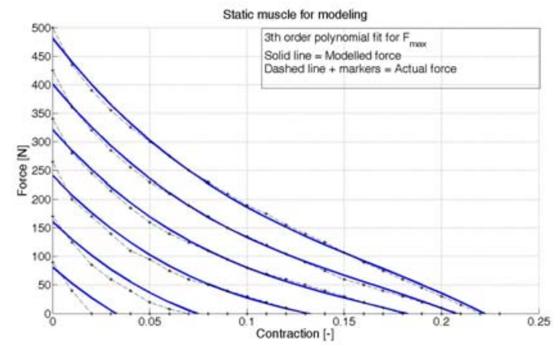

Fig. 3. Static muscle force modeling

Figure 3 shows the predicted force plotted against the force data provided by the manufacturer, at different pressure levels (0.1 to 0.6 MPa). For estimating the maximum force (F_{max}) in equation (7), a fourth-order polynomial curve fit was used. The model is able to predict the force reasonably well for almost every pressure. Some deterioration exists between the model and actual data only at lower pressure levels (less than 0.2 MPa). Also, it should be noted that our model does not take into account the hysteresis effect caused by inherent friction. In Festo fluidic muscles, the hysteresis is reported to be approximately 5% [40]. This adds to the uncertainties in the overall system model. Various approaches have been attempted to describe the dynamic characteristics of the muscle actuator. A common way is to treat the pneumatic muscle as a spring-mass-damper system. This method requires experimentation in order to obtain the stiffness and damping coefficients. The muscle damping coefficient is difficult to determine exactly, such that a constant approximation of it is included in the friction model.

Pressure Dynamics

Knowledge of the actual pressure inside the muscle is essential for understanding the dynamic behavior. The pressure depends on the quotient amount of air and volume of the muscle. The diameter and length of the muscle were measured, and the volume of the muscle was calculated assuming a cylindrical shape of the actuator. The volume shows a nearly linear behavior, dependent on displacement:

$$V_m(x) = v_0 + v_1 x, \tag{9}$$

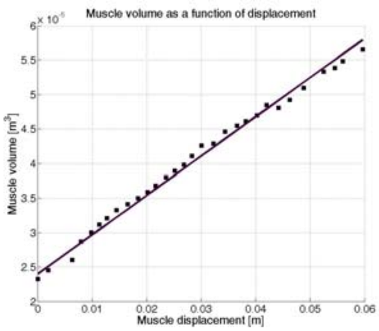

Fig. 4. Muscle volume in correlation with displacement

For calculating the pressure inside the muscle, it is assumed that the air is ideal gas and the change of air is isothermal, such that the pressure change can be expressed as follows:

$$\dot{p}_m = \frac{1}{V_m}\left(RT\dot{m}_g - p_m\dot{V}_m\right) \tag{10}$$

Where ρ, R, T, V_m and m_g denote the specific heat ratio density, gas constant, temperature, volume of the muscle, and gas mass, respectively. The expression inside the bracket of equation (10) considers the power balance of the pressurized flow rate. The first term inside the bracket gives the pressure change due to the mass flow in or out of the muscle chamber. The second term considers the pressure change due to the change of the muscle chamber volume. The reciprocal volume before the bracket takes into account the compressibility of the gas.

High Speed Valve Modeling

The mass flow rate model of the 3/2 high speed on/off valve is an essential part of the system model. Based on isentropic flow assumptions, the mass flow rate dm_g/dt through a valve orifice with an effective area A_v has to be treated as compressible and turbulent. If the upstream to downstream pressure ratio is larger than a critical pressure ratio p_{cr} the flow will attain sonic velocity (choked flow) and will depend linearly on the upstream pressure. If the pressure ratio is smaller than critical value the mass flow depends nonlinearly on both pressures. The standard equation for the mass flow rate may be expressed as follows [47]:

$$\dot{m}(p_u, p_d) = \begin{cases} \sqrt{\frac{k}{RT}\left(\frac{2}{k+1}\right)^{\frac{k+1}{k-1}}}\; C_f p_u A_v & if\ \frac{p_d}{p_u} \le p_{cr} \\ \sqrt{\frac{2k}{RT(k-1)}}\sqrt{1-\left(\frac{p_d}{p_u}\right)^{\frac{k-1}{k}}}\; \left(\frac{p_d}{p_u}\right)^{\frac{1}{k}} C_f p_u A_v & if\ \frac{p_d}{p_u} \succ p_{cr} \end{cases} \tag{11}$$

Where C_f is a non-dimensional discharge coefficient, p_u is the upstream pressure, and p_d is the downstream pressure. The meaning of the upstream and downstream pressure is different for the charging and discharging process of the muscle chamber. For charging, the valve is actuated and the supply pressure is considered the upstream pressure, and the muscle pressure is the downstream pressure. For discharging, the valve is closed and the muscle pressure is upstream pressure and the ambient pressure is the downstream pressure.

The 3/2-on/off solenoid valve is controlled with the duty cycle of the PWM-modulated signal. The time period of the PWM-signal is determined as T_{PWM} and is the inverse of the switching frequency $T_{PWM}=1/f_{PWM}$. The switching time for opening and closing the valve is approximately 2 ms, which reduces the maximum available duty cycle range. The switching frequency and the duty cycle determine how long the valve is open and closed during time period T_{PWM}. Valve delays and the discontinuous high frequency switching increase the complexity of the valve model, and are difficult to handle in the view point of controller design. Thus, an alternative valve model is needed for controller design. In a PWM-controlled system, the power is delivered to the actuator in discrete packets of fluid mass, as the valve is either completely open (on) or closed (off). If the switching frequency of the valve is significantly higher than the system dynamics, the system responds similarly as in the case of continuous mass flow. As the control signal for the valve is actually the duty cycle, it is necessary to determine the average mass flow rate as a function of muscle pressure and duty cycle control signal.

In this case, a similar procedure is followed as was introduced in [48], where the mass flow rate model was determined for a proportional servo valve. The equivalent mass flow rate has nonlinear characteristics and is a function of pressure p_m inside the muscle, and the control signal u (duty cycle). Thus, one obtains the representation for the pressure change as follows:

$$\begin{aligned} \dot{p}_m &= \frac{kRT}{V_m(x)}\dot{m}_{eq}(u, p_m) - \frac{kp}{V_m(x)}\frac{dV_m(x)}{dx}\dot{x} \\ \Rightarrow \dot{p}_m &= f_1(x, p_m, u) + f_2(x, p_m, \dot{x}) \end{aligned} \tag{12}$$

In equation (12), the second term can be computed once the muscle volume is V_m is known, and the muscle pressure is given. In the first term, the nonlinear valve function is difficult to measure. Alternatively, the nonlinear valve characteristic can be approximated experimentally by inflating and deflating a constant volume which causes the second term in equation (12) to disappear. A set of input signals with different duty cycles were applied to the valve and the pressure response in the constant chamber was measured. It is obvious that due to high frequency switching, the pressure signal contains a significant amount of vibrations. Thus, the pressure response requires filtering in order to obtain an averaged response. The average pressure signal may then be differentiated in order to obtain the pressure change at different times. By distributing the computed slopes of the pressure curve at the corresponding parameter pairs (u and p_m), a parametric representation of the surface of the pressure change can be obtained. Using this surface, the mass flow rate can be estimated using equation (13). Figure 5 shows the estimated mass flow rate plotted as a function of input signal (duty cycle) and the muscle pressure.

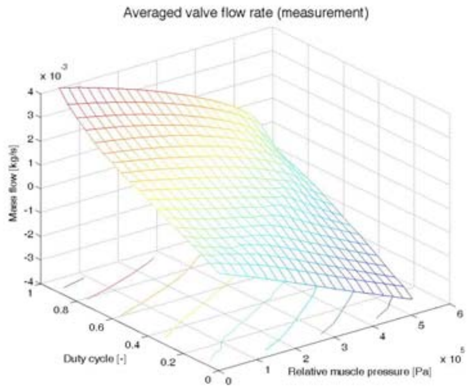

Fig. 5. Estimated mass flow rate for on/off valve

In order to estimate the mass flow rate, a 2nd order bi-polynomial function was used, as follows:

$$\dot{m}_{eq}(u, P_m) = m_1 + m_2 P_m + m_3 P_m^2 + m_4 u + m_5 u P_m + m_6 u P_m^2 + m_7 u^2 + m_8 u^2 P_m + m_9 u^2 P_m^2 \tag{13}$$

Where $m_{1\text{-}9}$ are the coefficients found using the least squares method. The output obtained from this function is plotted in Fig. 6. It can be observed that the model approximates the averaged mass flow rate behavior of the valve quite well.

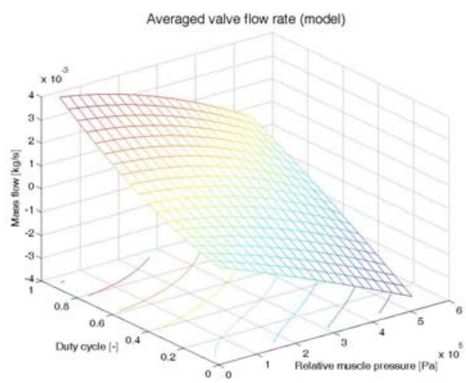

Fig. 6. Fitted model for mass flow rate

Overall Model

The motion equation of the muscle driving a constant payload attached in a vertical direction is defined (using Newton's Second Law) as follows:

$$M\ddot{x} = F_m - F_f - Mg \tag{14}$$

Where F_m is the static muscle force, F_f is the friction force, M is the total mass of the system and payload, and g is the gravitational constant. The frictional force F_f of the system is supposed to be a viscous friction (damping) of the muscle actuator, defined by:

$$F_f = B\frac{dx}{dt} \tag{15}$$

Where B is an experimentally approximated damping factor of the muscle actuator. Furthermore, suppose that the state vector for the system is defined as follows:

$$x_{states} = [P_m \quad x \quad \dot{x} \quad \ddot{x}]^T \tag{16}$$

From the nonlinear models described in the previous sections (particularly equations (12) and (14)), we have the following discrete-time equations which are used in the control and estimation processes:

$$x_{1,k+1} = \frac{\gamma T_S}{v_0 + v_1 x_{2,k}}[RTf(u, x_{1,k}) - x_{1,k} v_1 x_{3,k}] + x_{1,k} \tag{17}$$

$$x_{2,k+1} = T_S x_{3,k+1} + x_{2,k} \tag{18}$$

$$x_{3,k+1} = \frac{T_S}{M}[f(x_{2,k}) - (P_{\max} - x_{1,k})\frac{k_0 - k_1 x_{2,k}}{k_2} - Bx_{3,k} - Mg] + x_{3,k} \tag{19}$$

$$x_{4,k+1} = \frac{x_{3,k+1} - x_{3,k}}{T_S} \tag{20}$$

Furthermore, note that the measurement equation is defined as follows (only pressure and position measurements are available):

$$z_{k+1} = \begin{bmatrix} 1 & 0 & 0 & 0 \\ 0 & 1 & 0 & 0 \end{bmatrix} x_{k+1} \tag{21}$$

SLIDING MODE CONTROLLER AND FILTER

SMC Design

SMC is a form of variable structure control, which utilizes a discontinuous switching plane along some desired trajectory [22, 23]. This plane is often referred to as a sliding surface, in which the objective is to keep the state values along this surface by minimizing the state errors (between the desired trajectory and the estimated or actual values). Ideally, if the state value is off or away from the surface, a switching gain would be used to push the state towards the sliding surface. Once upon the surface, the motion of the system as the states slide along the surface is called a sliding mode [23]. The switching brings inherent stability to the control strategy, while also introducing excessive chattering (high-frequency switching) which is undesirable in practice and can excite unmodeled dynamics. A boundary layer may be introduced along the sliding surface in order to saturate and smooth out the chattering within the boundary region.

The SMC design is based on the nonlinear system model. Since the SMC design allows for model uncertainty, the stick-slip and Coulomb friction components are neglected in the model such that the friction is described only with viscous friction, as per equation (15). Substituting the muscle static force equations (7) and (8), and friction equation (15) into equation (14), and taking the derivative yields:

$$\dddot{x} = \frac{1}{M}\left[U(u_{eq}, x, p_m) + H(x, \dot{x}, p_m) - B\ddot{x}\right] \tag{22}$$

Where the above terms are defined by:

$$U(u_{eq}, x, p_m) = \left[\frac{kRT}{V_m(x)}\dot{m}_{eq}(u_{eq}, p_m) - \frac{kp_m\dot{V}_m(x)}{V_m(x)}\right]\left(\frac{k_0 - k_1 x}{k_2}\right) \quad (23)$$

$$H(x, \dot{x}, p_m) = \left(a_1 + 2a_2 x + 3a_3 x^2 + (p_{\max} - p_m)\frac{k_1}{k_2}\right)\dot{x} \quad (24)$$

Applying the equivalent control design method from [23] yields the following sliding surface definition:

$$S = \ddot{x} - \ddot{x}_d + 2\lambda(\dot{x} - \dot{x}_d) + \lambda^2(x - x_d) \quad (25)$$

The purpose of the equivalent control signal is to keep the system state on the sliding surface after it has reached it. The state will stay on the surface when *dS/dt=0*, which gives the equivalent control value *U*:

$$\begin{aligned} U(u_{eq}, x, p_m) &= -H(x, \dot{x}, p_m) + B\ddot{x} \\ &\quad + M(\ddot{x}_d - 2\lambda(\ddot{x} - \ddot{x}_d) + \lambda^2(\dot{x} - \dot{x}_d)) \end{aligned} \quad (26)$$

The desired equivalent mass flow rate through the valve can be solved using equation (26), as follows:

$$\dot{m}_{eq}(u_{eq}, p_m) = U(u_{eq}, x, p_m)\frac{V_m(x)}{kRT}\left(\frac{k_2}{k_0 - k_1 x}\right) + \frac{p_m\dot{V}_m(x)}{RT} \quad (27)$$

The remaining step is to convert the desired mass flow rate into the correct input signal (duty cycle value). Recall the second order bi-polynomial fitting equation (13), with the given values for the mass flow rates and the pressure measurement. The bi-polynomial equation reduces to the following quadratic equation in *u*:

$$C_{21}u^2 + C_{11}u + C_{01} = 0 \quad (28)$$

Where the parameters are defined by:

$$\begin{aligned} C_{01} &= m_1 + m_2 p_m + m_3 p_m^2 - \dot{m}_{eq} \\ C_{11} &= m_4 + m_5 p_m + m_6 p_m^2 \\ C_{21} &= m_7 + m_8 p_m + m_9 p_m^2 \end{aligned} \quad (29)$$

The correct value for desired input signal was determined to be the most positive root, as follows [48]:

$$u_{eq} = \frac{-C_{11} + \sqrt{C_{11}^2 - 4C_{21}C_{01}}}{2C_{21}} \quad (30)$$

Due to the numerical errors in the solution, the equivalent input control signal is bounded between 0 and 1 (as per the duct cycle signal which controls the valve). The SMC provides an input for the system of the following form:

$$u = u_{eq} + u_{sw} \quad (31)$$

The switching component of the input is defined as follows (where k_{SMC} is the switching gain, and φ is the boundary layer width):

$$u_{sw} = -k_{SMC}\,sat(s/\varphi) \quad (32)$$

Smooth Variable Structure Filter

In 2002, the variable structure filter (VSF) was introduced as a new predictor-corrector method used for state and parameter estimation [49, 50]. It is a type of sliding mode estimator, where gain switching is used to ensure that the estimates converge to true state values. An internal model of the system, either linear or nonlinear, is used to predict an a priori state estimate. A corrective term is then applied to calculate the a posteriori state estimate, and the estimation process is repeated iteratively. The SVSF was later derived from the VSF, and uses a simpler and less complex gain calculation [37]. In its present form, the SVSF is stable and robust to modeling uncertainties and noise, given an upper bound [37]. The basic concept of the SVSF is shown in Fig. 7. Assume that the solid line in Fig. 7 is a trajectory of some state (amplitude versus time). An initial value is selected for the state estimate. The estimated state is pushed towards the true value. Once the value enters the existence subspace, the estimated state is forced into switching along the system state trajectory [37].

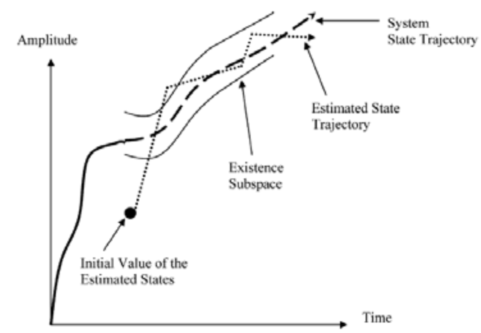

Fig. 7. SVSF Estimation Concept [37]

The SVSF method is model based and applies to smooth nonlinear dynamic equations. The estimation process may be summarized by equations (33) to (36), and is repeated iteratively. An a priori state estimate is calculated using an estimated model of the system. This value is then used to calculate an a priori estimate of the measurement, defined by equation (34). A corrective term, referred to as the SVSF gain, is calculated as a function of the error in the predicted output, as well as a gain matrix and the smoothing boundary layer width. The corrective term calculated in equation (35) is then used in equation (36) to find the a posteriori state estimate.

$$\hat{x}_{k+1|k} = \hat{F}(\hat{x}_{k|k}, u_k) \quad (33)$$

$$\hat{z}_{k+1|k} = \hat{C}\hat{x}_{k+1|k} \quad (34)$$

$$K_{k+1} = \hat{C}^{-1}\left|\left(\left|e_{z_{k+1|k}}\right|_{ABS} + \gamma\left|e_{z_{k|k}}\right|_{ABS}\right)\right|_{ABS} \circ sat(e_{z_{k+1|k}}, \Psi) \quad (35)$$

$$\hat{x}_{k+1|k+1} = \hat{x}_{k+1|k} + K_{k+1} \quad (36)$$

$$e_{z_{k|k}} = z_k - \hat{z}_{k|k} \quad (37)$$

$$e_{z_{k+1|k}} = z_{k+1} - \hat{z}_{k+1|k} \quad (38)$$

Two critical variables in this process are the a priori and a posteriori output error estimates, defined by equations (37) and (38), respectively [37]. Note that equation (37) is the output error estimate from the previous time step, and is used only in the gain calculation.

Sliding Mode Controller and Filter Strategy

The estimated states from the SVSF are used by the sliding mode controller to obtain a discontinuous control signal. This signal drives the plant to follow a desired state trajectory required by the pneumatic McKibben muscle actuator. This control strategy may be summarized as follows (assuming some initial values):

1. The uncertain system model is used to determine the *a priori* state and measurement estimates (equations (33) and (34)).
2. Estimated and measured state values are used to calculate the error (equations (37) and (38), depending on the time step).
3. The SVSF corrective gain is calculated as a function of the errors (equation (35)).
4. The *a posteriori* estimates are formed based on the corrective gain (equation (36)).
5. The updated estimates and desired state values are fed into the SMC, where the sliding surface (equation (25)) and equivalent control (equation (30)) are calculated.
6. As per the SMC strategy, an input is calculated based on the equivalent input and the switching component (equation 32).
7. Based on this control input, the system (plant) model is controlled and new measurements are taken. These measurements are then used at the start of the process (step 2), after the new *a priori* state estimates have been calculated.

The above process is iteratively repeated until the end of the desired trajectory tracking process.

SIMULATION RESULTS AND DISCUSSION

This section describes the results of simulating the SMC-SVSF strategy on the aforementioned system models for following a desired state trajectory. The following equation describes the desired position for the muscle actuator:

$$x_d = A\sin(2\pi ft) \tag{39}$$

Where A refers to some desired amplitude (0.02 m in this case), f is the frequency of vibration (0.2 Hz), and t is the simulation time (up to 10 seconds). The payload mass (M) used in the simulation was 10 kg. The desired velocity and accelerations are simply the corresponding derivatives of equation (39). Gaussian measurement noise added to the simulation was 10 kPa for the pressure sensor, and 0.1 mm for the measurement sensor. The SMC gain was set to a constant 20, the boundary layer was defined as 125, and the break-frequency (λ) used was 75. For the SVSF, the constant diagonal gain value (γ, used in the SVSF gain calculation) was set to 0.2, and the boundary layers for the states were defined as 1300, 250, 200, and 200, respectively (as per equation (16)). These values were obtained by trial-and-error.

The estimated pressure was calculated quite well. In fact, as shown in Fig. 8, it is nearly impossible to differentiate between the measured and estimated pressures.

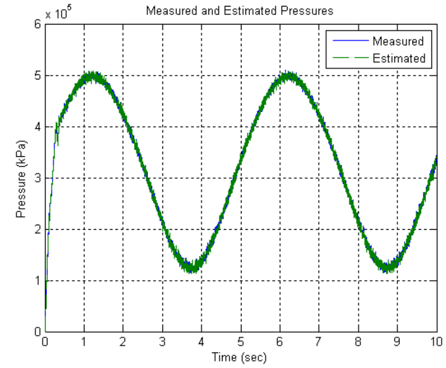

Fig. 8. Measured and estimated pressures

The desired, measured, and estimated positions are shown in Fig. 9. After less than half a second, the measured position was very close to the desired trajectory. The initial measured and estimated position were clearly set to 0 m, which caused the delay in reaching the desired trajectory, which immediately demanded 0.0225 m at the start of the simulation (this is akin to a step input). Note that there is no overshoot present when the trajectory is reached, and there appears to be no steady state errors.

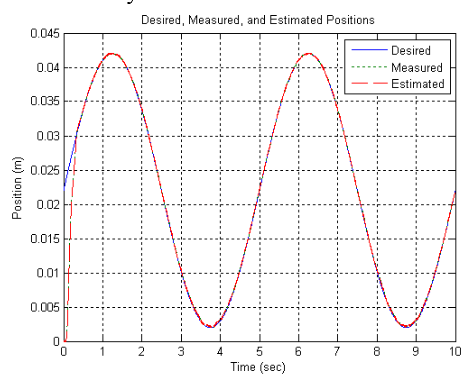

Fig. 9. Desired, measured, and estimated positions

Figure 10 shows the error between the desired and estimated position (note the scale). The position error ranges between 0.1 mm and about -0.3 mm. Clearly this is well within acceptable ranges, and demonstrates the effectiveness of this control strategy.

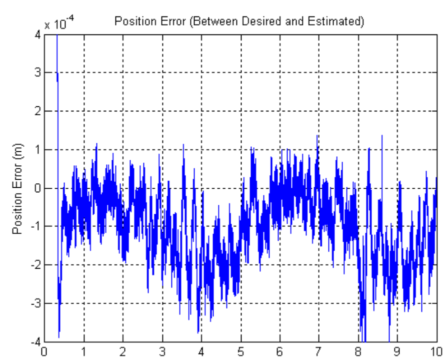

Fig. 10. Position error (between desired and estimated)

Furthermore, the demanded and estimated velocities are shown to be fairly close. Larger errors existed (and were expected) due to the fact that no measurements were available for the velocity. The velocity estimate had to be extracted based on a relationship with the pressure and position measurements found within the system model. That being said, however, the results are still quite reasonable.

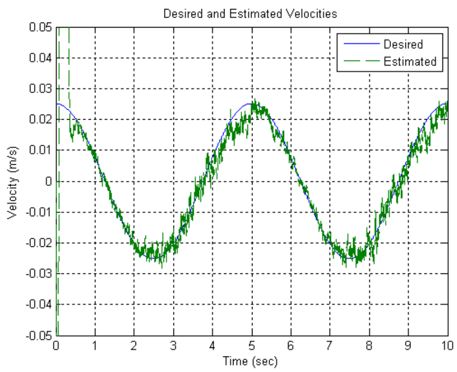

Fig. 11. Desired and estimated velocities

The results of the SMC-SVSF control strategy were also compared with a tuned PID controller. The PID was tuned to 50, 80, and 0.1 for the proportional, integral, and derivative gains, respectively. Figure 12 shows the comparison of the position results between the two methods.

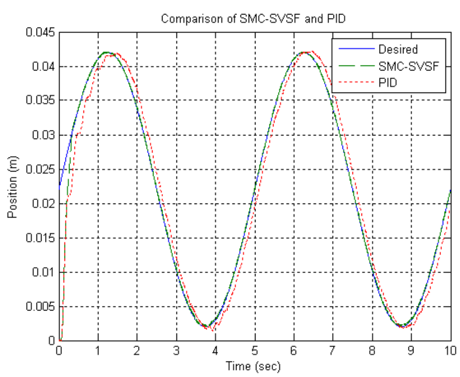

Fig. 12. Comparison of SMC-SVSF and PID positions

The root mean squared errors (RMSE) were calculated for both strategies. The RMSE for the PID was 0.0018 m (or 1.8 mm), and the RMSE for the SMC-SVSF was calculated to be 0.00014 m (or 0.14 mm). Clearly the SMC-SVSF strategy outperforms when compared with the PID method.

CONCLUSIONS

In this paper, a robust and stable control strategy was applied to a model of a Festo fluidic muscle actuator. The main objective of this application was trajectory following control. A complete model of this system was not available, and not all of the states had corresponding measurements. As such the SVSF was used to provide full-state information for those states without measurements. A new strategy that combines SMC with SVSF was used to control this system. The inherent robustness of the SMC-SVSF method is one of its main advantages over other controllers. The described control strategy was found to overcome the nonlinearities present in the system, has a fast response time, and is robust and stable to modeling uncertainties and measurement noise.

NOMENCLATURE

A_v	[m^2]	effective orifice area of the valve
B	[Ns/m]	viscous friction coefficient
C_f	[-]	discharge coefficient of the valve
D, D_0	[m]	muscle actuator diameter
F	[N]	force
F_{max}	[N]	maximum muscle force muscle
F_{muscle}	[N]	force generated by the muscle
K	[-]	SVSF gain
L	[m]	muscle actuator length
M	[kg]	weight of the payload
p_m	[Pa]	pressure inside the muscle
p_0	[Pa]	atmosphere pressure
p_s	[Pa]	supply pressure
R	[J/(kgK)]	gas constant
S	[-]	sliding surface
T	[K]	air temperature
T_{PWM}	[s]	time period of PWM-signal
T_S	[s]	sampling time (0.001 sec)
V	[m^3]	volume
V_m	[m^3]	volume of the muscle
$a_{0\text{-}3}$	[m]	muscle force coefficients
b_s	[m]	length of one braid strand
f_{PWM}	[Hz]	switching frequency of the PWM-signal
g	[m/s^2]	gravity constant
k_{SMC}	[-]	SMC gain
k	[-]	specific air heat ratio
k_0	[N]	coefficient for muscle force eq.
k_1	[N/m]	coefficient for muscle force eq.
k_2	[Pa]	coefficient for muscle force eq.
l	[m]	muscle length
l_0	[m]	muscle initial length
$\dot{m}_{eq}$	[kg/s]	equivalent mass flow rate
$\dot{m}_g$	[kg/s]	mass flow rate
$m_{1\text{-}9}$	[-]	coefficients for eq. mass flow rate
n_s	[-]	number of strand encircles
p	[Pa]	pressure
p_{cr}	[Pa]	critical pressure ratio
p_d	[Pa]	valve downstream pressure
p_m	[Pa]	pressure inside the muscle
p_{max}	[Pa]	maximum muscle pressure
p_0	[Pa]	atmosphere pressure
p_u	[Pa]	valve downstream pressure
u	[-]	control signal (duty cycle ratio)
u_{eq}	[-]	equivalent control signal
x	[m]	displacement of the muscle
θ, θ_0	[º]	muscle braid angle, initial braid angle
φ	[-]	SMC boundary layer thickness
γ	[-]	constant diagonal gain (between 0 and 1)
Ψ	[-]	SVSF boundary layer thickness
ε	[-]	muscle contraction ratio
λ	[-]	break-frequency of SMC filter

ρ	[kg/m^3]	gas density
v_0, v_1,	[m^3, m^2]	muscle volume coefficient
^	[-]	denotes and estimated value
~	[-]	denotes an error value
·	[-]	denotes a time derivative

REFERENCES

[1] Caldwell, D.G., Medrano-Cerda, G.A, and Goodwin, M.J., Braided pneumatic actuator control of a multi-jointed manipulator, Proceedings of the IEEE International Conference on Systems, Man and Cybernetics, pp. 423–428, Le Touquet, 1993.

[2] Caldwell, D.G., Medrano-Cerda, G.A, and Goodwin, M.J., Characteristics and adaptive control of pneumatic muscle actuators for a robotic elbow, Proceedings of the 1994 IEEE International Conference on Robotics and Automation, Vol. 4, May 1994, pp. 3558–3563.

[3] Caldwell D.G., Medrano-Cerda, G.A., and Goodwin, M.J., Control of Pneumatic Muscle Actuators, IEEE Control Systems Magazine, Vol. 15, No. 1, pp. 40–48, 1995.

[4] Medrano-Cerda, G.A., Bowler, C.J., and Caldwell, D.G., Adaptive position control of antagonistic pneumatic muscle actuators, IEEE/RSJ International Conference on Intelligent Robots and Systems, Vol. 1, pp. 378–383, Pittsburgh, PA, USA, 1995.

[5] Lilly, J., Adaptive tracking for pneumatic muscle actuators in bicep and tricep configurations, IEEE Trans. Neural Syst. Rehabil. Eng., Vol. 11, No. 3, pp. 333–339, Sep. 2003.

[6] Nagaoka, T., Konishi, Y., and Ishigaki, H., Nonlinear optimal predictive control of rubber artificial muscle, Proc. SPIE- Int. Soc. Opt. Eng., Vol. 2595, pp. 54–61, Oct. 1995.

[7] Hamerlain, M., Anthropomorphic robot arm driven by artificial muscles using a variable structure control, Proc. IEEE Int. Conf. Intelligent Robots Systems, Pittsburgh, PA, Aug. 1995, pp. 550–555.

[8] Repperger, D.W., Johnson, K.R., and Phillips, C.A., A VSC position tracking system involving a large scale pneumatic muscle actuator, Proc. of the IEEE Conf. on Decision & Control, Vol. 4, pp. 4302–4307, 1998.

[9] Repperger, D.W., Phillips, C. A., and Krier, M., Controller design involving gain scheduling for a large scale pneumatic muscle actuator, Proc. IEEE Conf. Control Applications, Kohala Coast, HI, Aug. 1999, pp. 285–290.

[10] Hesselroth, T., Sarkar, K., Van der Smagt, P., and Schulten, K., Neural network control of a pneumatic robot arm, IEEE Trans. Syst., Man, Cybern. B, Cybern., Vol. 24, No. 1, pp. 28–38, 1994.

[11] Carbonell, P., Jiang, Z. P., and Repperger, D. W., A fuzzy backstepping controller for a pneumatic muscle actuator system, Proc. IEEE Int. Symp. Intelligent Control, Mexico City, Sep. 2001, pp. 353–358.

[12] Chan, S. W., Lilly, J., Repperger, D. W., and Berlin, J. E., Fuzzy PD+I learning control for a pneumatic muscle, Proc. 2003 IEEE Int. Conf. Fuzzy Systems, St. Louis, MO, May 2003, pp. 278–283.

[13] Chang, X., and Lilly, J. H., Tracking control of a pneumatic muscle by an evolutionary fuzzy controller, Intell. Automat. Soft Comput., Vol. 9, No. 3, pp. 227–244, Sep. 2003.

[14] Balasubramanian, K., and Rattan, K.S., Fuzzy logic control of a pneumatic muscle system using linearizing control scheme, International Conference of North American Fuzzy Information Processing Society, pp. 432-436, 2003.

[15] Balasubramanian, K., and Rattan, K.S., Feedforward control of a non-linear pneumatic muscle system using fuzzy logic, IEEE International Conference of Fuzzy Systems, Vol.1, pp.272-277, 2003.

[16] Cai, D., and Yamaura, H., A VSS control method for a manipulator driven by an artificial muscle actuator, Electron. Commun., Part 3, Vol.80, No. 3, pp.55–63, Japan, 1997.

[17] Tondu, B., and Lopez, P., Modeling and Control of McKibben Artificial Muscle, IEEE Control Systems Magazine, pp. 15–38, April 2000.

[18] Carbonell, P., Jiang, Z., and Repperger, D., Nonlinear control of a pneumatic muscle actuator: backstepping vs. sliding-mode, Proceedings of the 2001 IEEE International Conference on Control Applications, Mexico City, Mexico, pp. 167–172, Sept. 2001.

[19] Lilly, J.H., and Yang L., Sliding mode tracking for pneumatic muscle actuators in opposing pair configuration, IEEE Transactions on Control Systems Technology, Vol. 13, pp. 550–558, July 2005.

[20] Mihajlov, M., Hubner, M., Ivlev, O., and Gräser, A., Modeling and Control of Fluidic Robotic Joints with Natural Compliance, Proceedings of the 2006 IEEE International Conference on Control Applications, Munich, Germany, October 4–6, 2006, pp. 2498–2503.

[21] Arenas, J., Pujana-Arrese, A., Riano, S., Martinez-Esnaola, A., and Landaluze, J., Sliding mode position control of a 1-dof set-up based on pneumatic muscles.

[22] Utkin, V. I., Sliding Modes and Their Application in Variable Structure Systems, Moscow, Russia: MIR Publishers, 1978.

[23] Slotine, J.J., and Li, W., Applied Nonlinear Control. Englewood Cliffs, NJ: Prentice-Hall, 1991.

[24] Morita, Y.S., Shimizu, M., and Kagawa, T., An Analysis of Pneumatic PWM and its Application to a Manipulator, Proc. of International Symposium of FluidControl and Measurement, Tokyo, pp. 3–8, 1985.

[25] Noritsugu, T., 1986, Development of PWM Mode Electro-Pneumatic Servomechanism, Part I: Speed Control of a Pneumatic Cylinder, J. Fluid Control, 17–1, pp. 65–80.

[26] Noritsugu, T., 1986, Development of PWM Mode Electro-Pneumatic Servomechanism, Part II: Position Control of a Pneumatic Cylinder, J. Fluid Control, 17–2–, pp. 7–31.

[27] Lai, J.-Y., Singh, R., and Menq, C.-H, Development of PWM Mode Position Control for a Pneumatic Servo System, Journal of the Chinese Society of Mechanical Engineers, Vol. 13, No. 1, pp. 86–95, 1992.

[28] Kunt, C., and Singh, R., 1990, A Linear Time Varying Model for On-Off Valve Controlled Pneumatic Actuators, ASME J. Dyn. Syst., Meas., Control, 112–4, pp. 740–747.

[29] Ye, N., Scavarda, S., Betemps, M., and Jutard, A., 1992, Models of a PneumaticPWM Solenoid Valve for Engineering Applications, ASME J. Dyn.Syst., Meas., Control, 114–4, pp. 680–688.

[30] Messina, A., Giannoccaro, N.I., and Gentile, A., Experimenting and modeling the dynamics of pneumatic actuators controlled by pulse width modulated technique, Mechatronics, No. 15, pp. 859–881, 2005.

[31] Paul, A. K., Mishra, J. K., and Radke, M. G., 1994, Reduced Order Sliding Mode Control for Pneumatic Actuator, IEEE Trans. Control Syst. Technol., 2–30, pp. 271–276.

[32] Van Varseveld, R. B., and Bone, G. M., 1997, Accurate Position Control of a Pneumatic Actuator Using On/Off Solenoid Valves, IEEE/ASME Trans. Mechatron., 2–30, pp. 195–204.

[33] Barth, E. J., Zhang, J., and Goldfarb, M., 2003, Control Design for Relative Stability in a PWM-Controlled Pneumatic System, ASME J. Dyn. Syst., Meas., Control, 125–3, pp. 504–508.

[34] Shen, X., Zhang, J., Barth, E., and Goldfarb, M., Nonlinear averaging applied to the control of pulse width modulated (PWM) pneumatic systems, Proceedings of the American control Conference, pp. 4444–4448, Boston, 2004.

[35] Shen, X., Zhang, J., Barth, E., and Goldfarb, M., Nonlinear Model-Based Control of Pulse Width Modulated Pneumatic Servo Systems, Journal of Dynamic Systems, Measurement and Control, September 2006, Vol. 128, pp. 663–669.

[36] Taghizadeh, M., Ghaffari, A., and Najafi, F., A Linearization Approach in Control of PWM-Driven Servo-Pneumatic Systems, 40th Southeastern Symposium on Systems Theory (SSST), March 2008, pp. 395–399.

[37] Habibi, S., The Smooth Variable Structure Filter, Proceedings of the IEEE, Vol. 95, No. 5, pp. 1026–1059.

[38] Schulte, R.A., The characteristics of the McKibben artificial muscle, In the Applications of External Power in Prosthetics and Orthotics. Publ. 874, Nas-RC, pp. 94–115, 1962.

[39] Chou, P., and Hannaford, B., Measurement and Modeling of a McKibben Pneumatic Artificial Muscles, IEEE Transactions on Robotics and Automation, Vol. 12, No. 1, Feb 1996.

[40] Festo, Fluidic Muscle MAS, Festo Brochure, 2002.

[41] Gaylord, R. H., Fluid Actuated Motor System and Stroking Device, US Patent No. 2,844,126. July 22, 1958.

[42] Inoue, K., Rubbertuators and applications for robotics, In 4th International Symposium on Robotics Research, pp. 57–63, 1987.

[43] Klute, G. K., and Hannaford, B., Accounting for elastic energy storage in McKibben artificial muscle actuators, ASME Journal of Dynamic Systems, Measurement and Control, Vol. 122, 2000.
[44] Delson, N., Hanak, T., Loewke, K., and Miller, D.N., Modeling and implementation of McKibben Actuators for a Hopping Robot.
[45] Davis, S., and Caldwell, D. G., Braid effects on contractile range and friction modeling in pneumatic muscle actuators, The International Journal of Robotics Research, Vol. 25, No. 4, April 2006, pp. 359–369.
[46] Kerscher, T., Albiez, J., Zöllner, J. M., and Dillman, R., FLUMUT – Dynamic Modelling of Fluidic Muscles Using Quick-Releases, Proceedings of the 3rd International Symposium on Adaptive Motion in Animals and Machines, Illmenau, Germany, 2005.
[47] Shearer, J.L., Study of pneumatic processes in the continuous control of motion with compressed air (I, II), ASME Trans., pp.233–249, 1956.
[48] Rao, Z., and Bone, G. M., Nonlinear modeling and control of servo pneumatic actuators, IEEE Transactions on Control Systems Technology, Vol. 16, No. 3, pp. 562–569, May 2008.
[49] Habibi, S., Burton, R., and Chinniah, Y., Estimation Using a New Variable Structure Filter, Proceedings of the American Control Conference, Anchorage, May 8–10, 2002.
[50] Habibi, S., and Burton, R., The Variable Structure Filter, Journal of Dynamic Systems, Measurement, and Control, ASME, Vol. 125, pp. 287–293.